International Journal of Plasticity 105 (2018) 211–224

Contents lists available at ScienceDirect

International Journal of Plasticity

journal homepage: www.elsevier.com/locate/ijplas

Modelling of shock waves in fcc and bcc metals using a combined continuum and dislocation kinetic approach

Nenad Djordjevic[a,*], Rade Vignjevic[a], Lewis Kiely[a], Simon Case[b], Tom De Vuyst[a], James Campbell[a], Kevin Hughes[a]

[a] Brunel University London, Structural Integrity Theme/Mechanical and Aerospace Engineering, NSIRC, Cambridge, CB21 6AL, United Kingdom
[b] AWE Aldermaston, Reading RG7 4PR, United Kingdom

ARTICLE INFO

Keywords:
bcc tantalum
Dislocation dynamics
Shock loading
Plate impact tests
Equation of state
Finite elements

ABSTRACT

Recent experimental data has revealed that, over short time scales (on the nanosecond scale), during formation of a shock in metals, amplitude of the 'elastic' precursor greatly exceeds the Hugoniot elastic limit (HEL), before decaying to the level of the HEL. Standard continuum scale material models are unable to reproduce this behaviour. To capture this aspect of material behaviour in metals, physical effects related to high rate dislocation mechanics must be taken into consideration (Mayer et al., 2013) and included into the continuum scale material model. The constitutive model developed here is defined at the continuum level, where the evolution of plastic deformation is controlled with a system of equations for three microscale state variables, for each slip system of a single crystal. These three state variables are the density of mobile dislocations, the density of immobile dislocations and the mobile dislocation velocity. The density evolutions of mobile and immobile dislocations are controlled by dislocation kinetic equations, which account for the generation of new dislocations, immobilisation of mobile dislocations and annihilation of dislocations. Dislocation velocity is determined by integration of the equations of motion of the mobile dislocations. The dislocation micromechanics is incorporated into the continuum model using the generalised Orowan equation, which relates plastic strain rate to the density of mobile dislocations and the velocity of mobile dislocations. Evolution of the yield surface is controlled by density of immobile dislocations.

The dislocation mechanics model (Krasnikov et al., 2011, Mayer et al., 2013) was combined with the orthotropic continuum scale material model (Vignjevic et al., 2012) with a vector shock equation of state (EOS) (Vignjevic et al., 2008), which was developed for modelling the response of orthotropic metals to high strain rate loading including presence of shockwaves. The continuum model was implemented in the LLNL Dyna3d (Liu, 2004) for linear solid elements.

Model validation was performed by comparison of numerical results with experimental data for plate impact tests (uniaxial strain state) for aluminium (fcc), copper (fcc) and tantalum (bcc). The numerical results show that during the first 50ns after impact, the pre-cursor wave has an amplitude similar to the stress level behind the shock front and relaxes to HEL with time (wave propagation). The difference between the experimental and numerical values of the compared variables (longitudinal stress, pulse length, elastic precursor relaxation time) was within 5% for the fcc materials, with the similar accuracy obtained for the bcc material, particularly for loading in the principal material direction.

* Corresponding author.
E-mail address: nenad.djordjevic@brunel.ac.uk (N. Djordjevic).

https://doi.org/10.1016/j.ijplas.2018.02.014
Received 27 October 2017; Received in revised form 20 February 2018; Accepted 22 February 2018
Available online 01 March 2018

1. Introduction

Accurate and reliable simulations of the high velocity impact loading can significantly reduce costs and the need for destructive testing during the design stages of many products, including aircraft, spacecraft, satellites, automobiles and weapons. The development of such simulations requires physical processes and properties of materials under loading to be accurately described mathematically. The model presented in this paper incorporates some of the main physical processes associated with plastic deformation of metals at extremely high strain rate loading.

The dynamic strength of metals, i.e. the stress required for plastic flow to occur, is observed to have a non-linear dependence on the strain rate (Qi et al., 2009) with the typical relationship between the dynamic strength and the strain rate shown in Fig. 1. Three regimes of strain rate dependence can be identified in this graph: regime 1, where an increase in strain rate produces very little increase in dynamic strength; regime 2, where an increase in strain rate produces a significant increase in dynamic strength; and regime 3, where an increase in strain rate produces very little increase in dynamic yield strength.

It is apparent from Fig. 1 that the strain rate dependence must be taken into account in the material model development and that the strain rate dependence can be a limiting factor in terms of the range of applicability of the model. The focus of this work is on modelling material behaviour at extremely high strain rates in the range of $10^6 s^{-1}$.

A number of models have been proposed to account for strain rate effects, starting from the early attempts by Johnson – Cook (Johnson and Cook, 1983), who developed a fully empirical model, with evolution of the yield surface controlled with the strain, strain rate and temperature effects. Another frequently used model is a semi empirical model developed by Steinberg and Guigan (Steinberg et al., 1980; Steinberg and Lund, 1989), which has been used in some recent developments, see for instance (Colvin et al., 2009). More recent significant developments are physically based models by Zerilli – Armstrong (Zerilli and Armstrong, 1987) and Follansbee – Kocks (Follansbee and Kocks, 1988). Zerilli – Armstrong is based on simple dislocation mechanics, with thermal activation of dislocations being the key process for plasticity evolution. This model uses distinct flow stress equations for the fcc and the bcc crystal structures, in order to accommodate the experimentally observed dissimilar effects of the strain, strain rate and temperature on the flow stress for these two structures. Mechanical Threshold Stress (MTS), model developed by Follansbee and Kocks, is also based on the thermal activation of dislocations. The flow stress in the MTS model consists of an athermal contribution and the temperature dependent contribution. The MTS model is of significant interest as the motivation of this work is to improve an existing in-house model (Vignjevic et al., 2012), which uses the MTS model for the yield surface evolution. More recent development of the models with thermally activated flow rules include (Khan et al., 2015; Khan and Liu, 2016) and (Hansen et al., 2013a,b).

However, the MTS and the other thermally activated flow models are limited to strain rates below $10^4 s^{-1}$, because the models are based on the assumption that the viscous drag effects are small in comparison to the dominant thermally activated dislocation motion (Banerjee and Bhawalkar, 2008), which is seen to only hold true for the strain rates up to $10^4 s^{-1}$.

During the formation of the shock waves in metals, elastic precursor decays in amplitude, from an initial amplitude similar to the plastic shock front, to the Hugoniot Elastic Limit (HEL) (Zhakhovsky et al., 2012). This behaviour occurs over short time scales and is widely explained as a consequence of insufficient number of mobile dislocations and the lack of dislocation mobility resulting in the high value of shear stress. Further, due to the very short time scales over which these phenomena occur, the relevant models need to be multiscale in nature in order to achieve the resolution required to reproduce this in the framework of continuum mechanics. This is due to the time and length scale ranges over which different types of modelling are applicable, as illustrated in Fig. 2. This suggests that plasticity models based on dislocation dynamics and an Orowan type relation provide potential for accurate representation of the precursor behaviour. Orowan relation defines rate of plastic strain at the continuum scale, using the density of mobile dislocations, velocity of moving dislocations and Burgers vectors.

A comprehensive review of the available material models identified a number of recently developed multiscale models based on the dislocation dynamics approach, including the single crystal models for fcc structures presented in (Groh et al., 2009; Colvin et al., 2009; Austin and McDowell, 2011; Hansen et al., 2013a; Mayer et al., 2015; Luscher et al., 2016; Mayeur et al., 2016) and the models developed for bcc crystal structures, see for instance (Ding and Asay, 2011; Asay et al., 2011). The models used the generalised

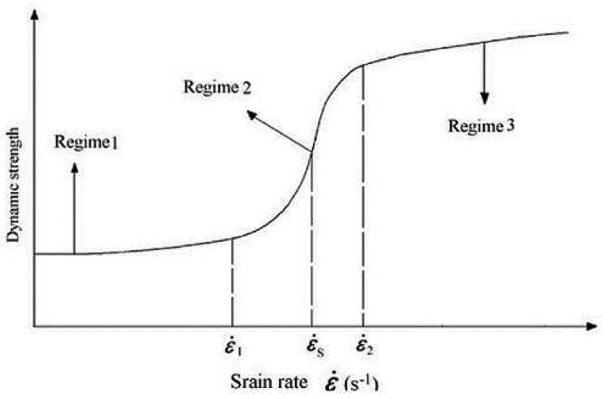

Fig. 1. Typical relationship between the dynamic strength and the strain rate for metals (Qi et al., 2009).

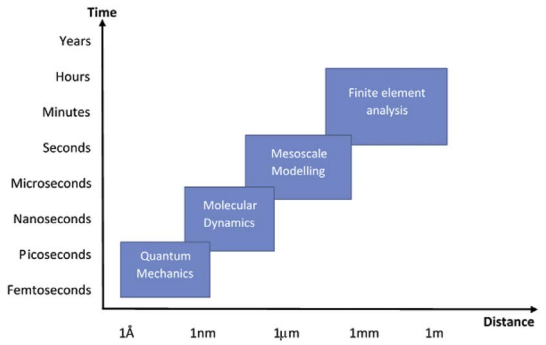

Fig. 2. Time and length scales applicable to different modelling methods.

Orowan's equation for bridging the dislocation scales to the continuum scale, with various ways of representing the evolution of physical deformation processes and calibrating of the material parameters in the model. For instance, Horstemeyer's group used bridging between the molecular dynamics and microscale discrete dislocation tool to predict the hardening law in the single crystal aluminium in (Groh et al., 2009). Colvin and co-authors implemented model in 2D radiation hydrocode with a dislocation density as an internal variable and provided a parametric study against the experimental data for Fe in (Colvin et al., 2009). Li and Zbib (Li et al., 2014) developed mechanism based dislocation dynamics model, controlled with two internal variables (mobile and immobile dislocation densities), which are determined from discrete dislocation dynamics. Austin and McDowell developed the model with two dislocation density variables, which was validated for extremely high strain rate loading featuring the shock amplitudes up to 10 GPa (Austin and McDowell, 2011, 2012). Similar approach was recently used in (Mayeur et al., 2016; Luscher et al., 2016). The model with three dislocation densities (mobile, pile up and debris) controlling the high strain rate loading of Cu was proposed by (Hansen et al., 2013a,b), where the focus was on the accurate prediction of transition from thermally activated regime (low strain rate) to the drag dominated dislocation motion typical for the high strain rates.

This literature review identified two models to be of particular interest to this work: a model developed by Malygin (1999) and a model developed by Krasnikov, Mayer and co-workers in (Krasnikov et al., 2010, 2011; Mayer et al., 2013; Yanilkin et al., 2014). Both models combine processes occurring at the microscale with the development of deformation at the continuum scale, using an Orowan's type relation. More importantly, the models predicted the decay in elastic precursor amplitude, which occurs during the shock wave formation in the metals. The key difference between the identified models is in the number of internal variables and their kinetic evolution equations, which determine the dislocations densities and dislocation velocities, which in turn constitute the generalised Orowan equation and the yield strength at the continuum level.

Consequently, the method proposed by Krasnikov, Mayer and co-workers (Krasnikov et al., 2011; Mayer et al., 2013) is selected as the most promising model, capable of reproducing the 'superelastic' precursor behaviour, for improvements to the existing in house high-strain rate orthotropic model. The performance of this model, for single crystal aluminium, is shown in Fig. 3, where the results for a symmetric plate impact test obtained with this model, are compared to the results of the equivalent problem modelled with the existing in house model (Vignjevic et al., 2012). The test was symmetric impact of two aluminium plates at a relative impact velocity of 500 m/s. The main difference between the results is in the amplitude of precursor obtained during the first 20ns of the shock formation: the results published in (Mayer et al., 2013) show that a plastic wave is formed in the material, with a decaying/relaxing precursor visible as the kink in the shock front. The results obtained with the in-house material model, shown in Fig. 3 b), feature the

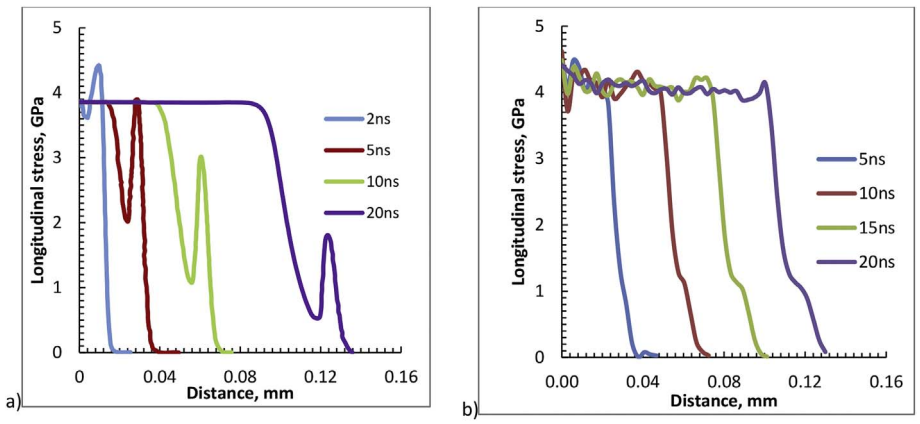

Fig. 3. Longitudinal stress versus distance into the target plate at several response times after impact at a relative impact velocity of 500 m/s: a) results obtained by Mayer (Mayer et al., 2013); b) the results obtained by existing in house model (Vignjevic et al., 2012).

precursor wave, with a fixed amplitude of approximately 1 GPa (HEL).

The main aim of this work is development of constitutive model capable of modelling elastic plastic behaviour of single crystal metals under extreme dynamic loading, including the shock wave formation and propagation, where the strain rates are of the order $10^6 s^{-1}$. The model combines the orthotropic continuum scale material model (Vignjevic et al., 2012) with a vector shock equation of state (Vignjevic et al., 2008), where the evolution of the plastic deformation is controlled by dislocation kinetic equations derived in (Krasnikov et al., 2011; Mayer et al., 2013) and used in the unchanged form, for each slip system of a single crystal. The model is implemented for linear solid elements in the Lawrence Livermore National Laboratories (LLNL) Dyna3d (Liu, 2004) and validated against available experimental data for the single crystal aluminium (Kanel et al., 2001), single crystal copper (Kanel et al., 1996; Krasnikov et al., 2011) and single crystal tantalum (Whiteman et al., 2014).

This paper consists of four sections: following the introduction to the problem given in Section 1, the constitutive model developed is described in Section 2, including its implementation given in Section 2.4. The numerical validation is given in Section 3, with the conclusions provided in Section 4.

2. Constitutive model

2.1. Continuum thermodynamics

In the framework of thermodynamics and configurational mechanics, kinematics of deformation at the continuum level is defined in terms of multiplicative decomposition of deformation gradient given as:

$$\mathbf{F} = \mathbf{F}_e\mathbf{F}_p \tag{1}$$

where: $\mathbf{F}_e$ represents thermo-elastic part of the deformation, and $\mathbf{F}_p$ represents the part of the deformation due to plastic deformation (dislocation mechanics). The decomposition (1) introduces an intermediate, elastically unloaded configuration, which is stress free at a reference temperature and can be physically obtained by elastic unloading of material. For the sake of compatibility with the orthotropic material formulation and the future use with the polycrystalline material structure, the proposed model is integrated in isoclinic intermediate configuration, which corresponds to the elastically unloaded configuration rotated back for the plastically induced rigid body rotation, as described in (Vignjevic et al., 2012) and illustrated in Fig. 4.

The material directions in the isoclinic configuration remain unchanged and corresponding multiplicative decomposition is defined as:

$$\mathbf{F} = \mathbf{F}_e\mathbf{F}_p = \mathbf{F}_e\mathbf{R}_p\mathbf{R}_p^T\mathbf{F}_p = \overline{\mathbf{F}}_e\overline{\mathbf{F}}_p \tag{2}$$

where polar decomposition of plastic part of deformation gradient defines the orthogonal tensor of rotation $\mathbf{R}_p$, which is used to obtain the elastic and plastic part of deformation gradient in isoclinic configuration: $\overline{\mathbf{F}}_e = \mathbf{F}_e\mathbf{R}_p$, $\overline{\mathbf{F}}_p = \mathbf{R}_p^T\mathbf{F}_p = \mathbf{R}_p^T\mathbf{R}_p\mathbf{U}_p = \mathbf{U}_p$. Green Lagrange strain pushed forward to the isoclinic configuration is additively decomposed as:

$$\overline{\mathbf{E}} = \overline{\mathbf{F}}_p^{-T}\mathbf{E}\overline{\mathbf{F}}_p^{-1} = \tfrac{1}{2}(\overline{\mathbf{F}}_e^T\overline{\mathbf{F}}_e - \mathbf{I}) + \overline{\mathbf{F}}_p^{-T}\Big(\tfrac{1}{2}(\overline{\mathbf{F}}_p^T\overline{\mathbf{F}}_p - \mathbf{I})\Big)\overline{\mathbf{F}}_p^{-1} = \overline{\mathbf{E}}_e + \overline{\mathbf{E}}_p \tag{3}$$

Equally, velocity gradient pulled back to the isoclinic configuration leads to additive decomposition defined as:

$$\overline{\mathbf{l}} = \overline{\mathbf{F}}_e^{-1}\mathbf{l}\overline{\mathbf{F}}_e = \overline{\mathbf{F}}_e^{-1}\dot{\overline{\mathbf{F}}}_e + \dot{\overline{F}}_p\overline{\mathbf{F}}_p^{-1} = \overline{\mathbf{l}}_e + \overline{\mathbf{l}}_p \tag{4}$$

where $\overline{\mathbf{l}}_e$ and $\overline{\mathbf{l}}_p$ are respectively elastic and plastic part of the velocity gradient in isoclinic configuration, which can be further divided into symmetric and antisymmetric/spin tensor. Evolution of elastic deformation is determined by elastic part of velocity gradient, whilst plastic part of velocity gradient determines the evolution of plastic deformation. The latter is calculated using the generalised Orowan's equation, which is described in the following subsection.

In the framework of thermodynamics, the velocity gradient in isoclinic configuration is work conjugate variable to Mandel stress $\overline{\boldsymbol{\Sigma}}$ (Mandel, 1972, 1974; Vignjevic et al., 2012), which is defined as a pull back of Kirchhoff stress $\boldsymbol{\tau}$, as:

$$\overline{\boldsymbol{\Sigma}} = \overline{\mathbf{F}}_e^T\boldsymbol{\tau}\overline{\mathbf{F}}_e^{-T} \tag{5}$$

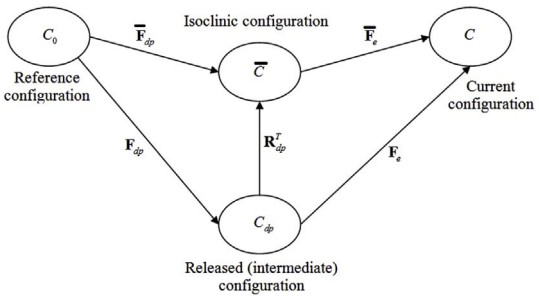

Fig. 4. Intermediate and isoclinic configurations for elastic plastic deformation obtained by multiplicative decomposition of deformation gradient.

Mandel stress tensor can be decomposed into the spherical and deviatoric part, which is in the tensor and the index notation, respectively given as:

$$\overline{\mathbf{\Sigma}} = -P\overline{\mathbf{\Psi}} + \overline{\mathbf{S}} \quad \overline{\Sigma}_{ij} = -P\overline{\psi}_{ij} + \overline{S}_{ij} \tag{6}$$

where P is pressure that is work conjugate to volumetric part of strain, $\overline{\psi}_{ij}$ is tensor determined by material elastic orthotropy (Vignjevic et al., 2008) with the following properties: $\overline{\psi}_{ij} \neq 0$ for $\forall \quad i = j$ and $\overline{\psi}_{ij} = 0$ for $\forall \quad i \neq j$; $\overline{S}_{ij}$ are components of deviatoric stress. Note that the tenor $\overline{\psi}_{ij}$ becomes δ_{ij} for the case of isotropic material formulation.

When modelling the shock response of materials, spherical part of the stress tensor is updated in the equation of state, whilst the deviatoric part is determined by the strength part of the constitutive model, where the assumption was made that only the elastic component of deviatoric part of the strain contributes to the deviatoric stress. Consequently, the generalised constitutive law can be written in the rate form as:

$$\dot{\overline{S}}_{ij} = C_{ijkl}\overline{d'}^{e}_{kl} \quad \dot{\overline{S}} = \mathbb{C}\overline{d'}_{e} \tag{7}$$

where Mandel stress is assumed to be symmetric (Vladimirov et al., 2009; Reese and Vladimirov, 2008), so that deviatoric part of elastic component of the rate of deformation, $\mathbf{d}'_e$ can be obtained from a symmetric part of the additively decomposed velocity gradient:

$$\overline{\mathbf{d}}'_e = (\overline{\mathbf{I}} - \overline{\mathbf{I}}_p)_{sym} - \frac{1}{3}\overline{\mathbf{d}}\colon \boldsymbol{\delta} \tag{8}$$

2.2. Dislocation based plasticity model

Plastic deformation is predominantly associated with the movement of dislocations under applied loading. This process, known as slip, occurs in specific directions within slip planes in the materials crystal structure. A slip direction is defined by the Burgers vector with the slip planes defined by a vector normal to the planes of closest packing. Making use of the conventional notation for the crystallographic planes (denoted in {}) and directions (denoted in ⟨⟩), the group of slip systems for face centred cubic (fcc) metals is defined with {111} slip planes and the ⟨110⟩ directions. There are four {111} planes, each having three ⟨110⟩ directions, resulting in a total of twelve combinations, or slip systems.

The body centred cubic (bcc) crystal are not as well defined, because there are no close packed planes in the bcc crystal, and the closest packed planes are generally considered to be the main slip planes. These are the six {110} planes with two directions being the ⟨111⟩, leading to twelve slip systems. In addition, some bcc materials have additional sets of slip systems due to the {112} and {123} planes also having at least one ⟨111⟩ direction. Since there are twelve {112} and twenty-four {123} planes each with one ⟨111⟩ direction, the bcc crystal poses a possible 48 slip systems.

Evolution of plastic deformation is modelled using the dislocation dynamics approach as proposed in (Krasnikov et al., 2011; Mayer et al., 2013) in unchanged form, so that the model is defined in terms of three internal state variables: density of mobile dislocations, density of immobile dislocations and velocity of mobile dislocations. Mobile dislocations are free to move in the crystal directions upon loading until they get blocked and become immobile dislocations or annihilate. Consequently, mobile dislocations control rate of plastic deformation, together with the dislocations velocity, whilst the permanently immobile dislocation density constitutes the yield strength.

Plastic strain in this model is calculated by integration of the rate of plastic deformation, given in terms of a generalised Orowan's equation:

$$d'^{pl}_{ij} = \frac{1}{2}\sum_{\beta}(b_i^{\beta}n_j^{\beta} + b_j^{\beta}n_i^{\beta})V_D^{\beta}\rho_D^{\beta} \tag{9}$$

Where: index β determines a slip system, V_D^{β} is the velocity of mobile dislocations, ρ_D^{β} is the density of mobile dislocations, and b_i^{β} and n_j^{β} are the Burger's vector and normal to the slip plane defining each slip system. The yield strength evolves according to the Taylor hardening relation (Krasnikov et al., 2011; Mayer et al., 2013), and uses the density of immobile dislocations as the main evolution variable:

$$Y = Y_0 + A_I G b\sqrt{\rho_I} \tag{10}$$

Here, Y_0 is the intrinsic lattice resistance and accounts for the Peierls stress, A_I is a dimensionless coefficient, G is the shear modulus, b is the magnitude of Burgers vector and ρ_I is the total density of immobile dislocations, calculated from the density of immobile dislocations for all slip systems:

$$\rho_I = \sum_{\beta}\rho_I^{\beta} \tag{11}$$

The densities of mobile and immobile dislocations are updated via the following dislocation kinetic equations proposed by Krasnikov, Mayer and co-workers in (Mayer et al., 2013):

$$\frac{d\rho_D^\beta}{dt} = Q_D^\beta - Q_I^\beta - k_a b|V_D^\beta|\rho_D^\beta(2\rho_D^\beta + \rho_I^\beta) \tag{12}$$

$$\frac{d\rho_I^\beta}{dt} = Q_I^\beta - k_a b|V_D^\beta|\rho_D^\beta\rho_I^\beta \tag{13}$$

$$Q_D^\beta = k_g b\left[\frac{2B(V_D^\beta)^2}{\sqrt{1-\left(V_D^\beta/c_t\right)^2}} + bY|V_D^\beta|\right]\rho_D^\beta \tag{14}$$

$$Q_I^\beta = V_I(\rho_D^\beta - \rho_0)\sqrt{\rho_I^\beta} \tag{15}$$

where Q_D^β and Q_I^β are respectively: rate of generation and rate of immobilisation; the k_a and V_I are respectively dislocation annihilation and the characteristic dislocations velocity during the consolidation, with the ρ_0 being the minimum density of mobile dislocations, which is required for their consolidation in the structure. The above equations account for the main dislocation density altering processes that are observed during plastic deformation. Three terms on the right hand side of equation (12) describe, respectively: the generation of new mobile dislocations, the immobilisation of mobile dislocations, and the annihilation of mobile dislocations with other mobile dislocations and immobile dislocations. The two processes governing the evolution of the immobile dislocation density are the immobilisation of mobile dislocations and the annihilation of immobile dislocations with mobile dislocations. The rate of generation of new mobile dislocations is calculated from the assumption that a certain portion of energy dissipated by plastic flow is used in the generation of dislocations. The parameter, k_g, termed the coefficient of generation, is defined as this fraction of dissipated energy divided by the energy required to form a dislocation in the metal, which when multiplied by the dissipated energy, results in the rate of dislocation generation. The term in the square brackets of equation (14) is simply work done by a dislocation overcoming resistance forces during slip.

The velocity of dislocations is determined by the means of equation of dislocation motion (Krasnikov et al., 2010, 2011; Mayer et al., 2013):

$$\frac{m_0}{\left(1-\left(V_D^\beta/c_t\right)^2\right)^{3/2}}\frac{dV_D^\beta}{dt} = \left[\sum_{i=1}^{3}\sum_{j=1}^{3}\overline{S}_{ij}b_i^\beta n_j^\beta \mp \frac{1}{2}bY\right] - \frac{BV_D^\beta}{\sqrt{1-\left(V_D^\beta/c_t\right)^2}} \tag{16}$$

where m_0 is the rest mass of dislocations per unit line, c_t is the transverse speed of sound, $\overline{S}_{ik}$ is the deviatoric stress tensor, and B is a coefficient of dynamic drag. The coefficient of dynamic drag is calculated as (Suzuki et al., 1991):

$$B = \frac{4\theta^2 k_b^3}{h^2 c_b^3}T \tag{17}$$

where: k_b and h are the Boltzmann constant and Planck's constant, respectively, c_b is the bulk speed of sound, θ is a temperature parameter similar to the Debye temperature and T is temperature.

The right hand side of the equation of dislocation motion (16), comprises terms that account for the forces acting on dislocations at stress levels associated with high strain rate deformation. Specifically, the first term of the right-hand side accounts for the mechanical force acting on dislocations per unit line. This force is resolved in the direction of the slip for each slip system by the lattice vectors. The second term on the right-hand side accounts for the yield resistance intrinsic in the material. It is a condition for slip to occur that the magnitude of the mechanical force must be greater than the magnitude of the yield resistance, with the minus/plus sign used to indicate that the resistance and mechanical force must always have opposite directions. The final term on the right-hand side describes the dynamic drag, which increases with increasing temperature and dislocation velocity. Dislocation self-forces are neglected here due to their small magnitude compared to the other forces at shock loading (Kosevich, 1965). Equation (16) closes the system of dislocation dynamics equations which are coupled with the continuum material scale through equations (9) and (10).

2.3. Evolution of the orientation of the slip systems

Slip systems defined for fcc and bcc crystalline structures are given in the reference/material configuration and remain unchanged upon mapping to the isoclinic configuration. Consequently, mapping of the lattice vectors, that define the slip systems in the current configuration, is defined making use of the multiplicative decomposition of deformation gradient (2) as:

$$\mathbf{b}^{*\beta} = \overline{\mathbf{F}}_e \cdot \mathbf{b}^\beta \tag{18}$$

$$\mathbf{n}^{*\beta} = \mathbf{n}^\beta \cdot \overline{\mathbf{F}}_e^{-1} \tag{19}$$

2.4. Model implementation

The model is implemented in explicit LLNL DYNA3d hydrocode (Liu, 2004) available at Brunel University London and coupled with vector Gruneisen EOS (Vignjevic et al., 2008). Deviatoric stress is updated by integration of the stress rate given in Equation (7), where the deviatoric part of rate of elastic deformation is obtained from Equation (8). Plasticity evolves when the trial stress is above the yield strength defined in Equation (10). When the plasticity criterion is met, the improved Euler method is used to numerically integrate equations (12)–(15) with the an analytical solution to Equation (16), available in (Krasnikov et al., 2011), used for dislocation velocity update. Finally, the plastic strain increment is obtained by using backward (implicit) Euler method for integration of (9).

3. Numerical validation

Numerical validation programme conducted in this work consists of three sets of tests, presented in separate sections below: 1) plate impact tests for fcc materials on aluminium and copper; 2) symmetric impact tests for single crystal aluminium; and 3) plate impact tests for bcc single crystal materials on tantalum.

3.1. FCC single crystal metals

Validation of the model for fcc single crystal material was performed by simulation of three plate impact tests for single crystal aluminium and copper. The plate impact test is a typical method for material characterisation under shock loading where a flyer plate impacts a target plate at a high velocity. Provided that contact between the flyer plate and target plate is ideally parallel, the material is in the uniaxial strain state leading to the formation of shock waves in both the target and the flyer plate (Meyers, 1994).

The plate impact tests model is illustrated in Fig. 5, with the symmetry boundary conditions applied to the free surfaces parallel to the loading direction. A 2.9 mm thick target plate is impacted by a 0.4 mm thick aluminium flyer plate at a velocity of 660 m/s. The model consists of a single, continuous mesh divided into two regions representing the flyer and the target. An initial velocity of 660 m/s is assigned to the flyer region, and the target region is initially stationary. This discretisation approach removes potential effects induced by the contact algorithms. The material axes are aligned with the element axes, so that impact in the z-direction corresponds to loading in [001] crystal direction.

The material model parameters required for modelling aluminium and copper are taken from (Krasnikov et al., 2011; Mayer et al., 2013) are given in Table 1, where ν is Poisson's ration and a is lattice parameter used for calculation of the Burger's vector. Parameters for the Gruneisen equation of state are taken from (Steinberg, 1991) and are summarised in Table 2.

Sensitivity of the numerical results to discretisation, time step size and artificial viscosity was analysed through a number of simulations performed for a range of mesh densities, with several combinations of the time step scale factors and linear and quadratic bulk viscosity coefficients. To capture the features of the physical process described above, the results presented were obtained with the element size of 1 μm, time scale factor equal to 0.1 and linear and quadratic bulk viscosity coefficients equal to 3.0 and 0.3, respectively.

Fig. 6 shows the rear surface velocity obtained for the aluminium plate impact simulations and compared with experimental data (Kanel et al., 2001; Mayer et al., 2013). The results show a good agreement for the initial acceleration, due to the precursor pulse, with the related sharp rise in the velocity accurately captured. The velocity pulse length at the rear surface was also accurately captured, with an apparent discrepancy between the slopes of the release waves.

The numerical results overestimate the velocity during the loading phase, with the calculated peak velocity being 4% greater than the experimentally observed values. This discrepancy could be attributed to a physical material property, or accuracy of experimental measurements. Although the simulation results follow the trend of the experimental curve, the release part of the curve in Fig. 6 shows a larger discrepancy, with the maximum difference between the two curves at one time instance being approximately 15%. This might be partly due to the fact that damage, i.e. deterioration of material properties, is not incorporated in the current version of the model. Alternatively, the shape of the release wave in the experimental results might be a consequence of pressure depended material constants, which is also not included in the current implementation of the model.

The material model was further validated against two copper plate impact tests in order to check the model performance at different loading rates. The first test was impact on a 0.7 mm thick copper target by 0.2 mm thick aluminium flyer, at the impact velocity of 560 m/s. The other experiment was impact at a 4.3 mm thick copper plate by a 0.4 mm thick aluminium flyer at 660 m/s. In both plate impact tests, the material axes are aligned with the global coordinate system to ensure an impact in the z-direction is parallel to the material crystal direction [001]. The rear surface velocity results for the copper plate impact tests are shown in Fig. 7.

Similar to the aluminium plate impact results, Fig. 7 also shows good agreement between the simulation results and experimental

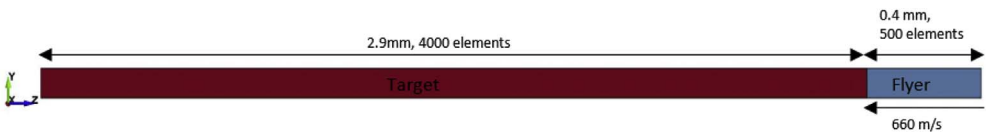

Fig. 5. Finite element model for aluminium plate impact tests.

Table 1
Material model parameters required for modelling aluminium and copper (Krasnikov et al., 2011; Mayer et al., 2013).

Model parameter	Aluminium	Copper
E	62.4 GPa	117.0 GPa
G	24.0 GPa	47.7 GPa
ν	0.340	0.337
ρ_0	10^7 cm^{-2}	10^7 cm^{-2}
k_g	7.9×10^{19} J^{-1}	7.9×10^{19} J^{-1}
k_a	10	10
A_I	6	4
V_I	5 ms-1	2 ms^{-1}
θ	430 K	280 K
Y_0	22 MPa	30 MPa
m_0	10^{-16} kgm^{-1}	10^{-16} kgm^{-1}
a	4.046 Å	3.610 Å

Table 2
Equation of state parameters for aluminium and copper (Steinberg, 1991).

Equation of state parameter	Aluminium	Copper
Velocity curve intercept, C	0.52 cm/μs	0.394 cm/μs
First slope coefficient, S_1	1.360	1.489
Gruneisen coefficient, γ_0	2.20	2.02
First order volume correction coefficient, a	0.48	0.47

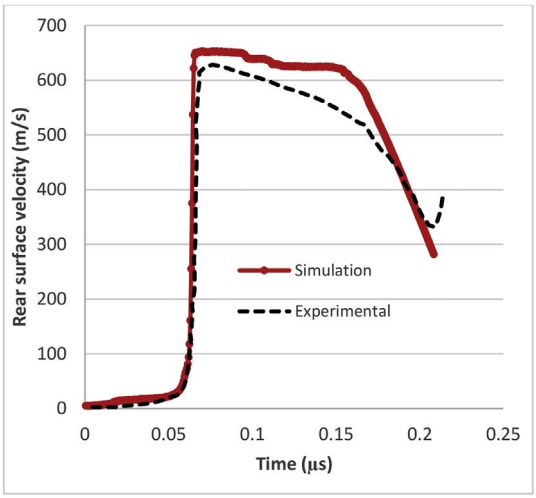

Fig. 6. Rear surface velocity of 2.9 mm thick aluminium target plate impacted by a 0.4 mm thick aluminium flyer plate at a velocity of 660 m/s; simulation results obtained with the model vs experimental data taken from (Kanel et al., 2001; Mayer et al., 2013).

data for the initial, precursor, pulse and the plastic shock front, with the even better agreement of the signal shapes and the peak rear surface velocity for the thinner target plate, see Fig. 7a. However, the simulation results for both cases overestimate the experimentally observed results in the unloading region, with the discrepancy more pronounced for the second impact case, conducted with the thicker plates (Fig. 7b).

The accurate capture of the initial segment of the rear surface velocity profiles for both aluminium and copper tests, particularly in terms of the acceleration, confirms the plasticity model works for fcc metals. The discrepancy between the unloading of the rear surface is consistent between both the aluminium and copper plate impact simulations and provide further indication of the need for the plasticity model to be coupled with an appropriate damage model.

3.2. Symmetric plate impact tests

The aim of the simulation of a symmetric plate impact test illustrated in Fig. 8 was to investigate the formation of the shock wave in the material and behaviour of the precursor wave. The simulation was set using a continuous mesh, divided into two regions of

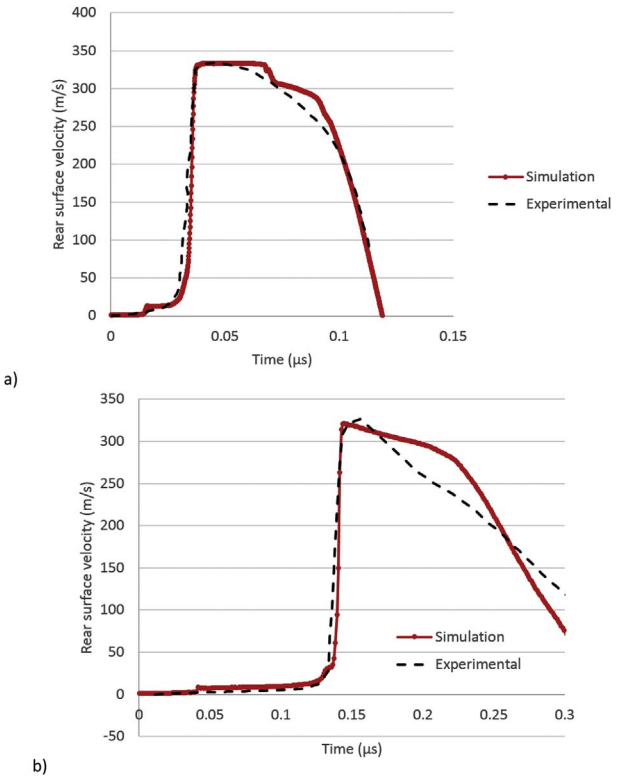

Fig. 7. Rear surface velocity profile: a) a 0.7 mm thick copper target impacted by a 0.2 mm thick aluminium flyer at a velocity of 560 m/s; b) a 4.2 mm thick copper target impacted by a 0.4 mm thick aluminium flyer at a velocity of 660 m/s; simulation results obtained with the model vs experimental data taken from (Kanel et al., 1996; Krasnikov et al., 2011).

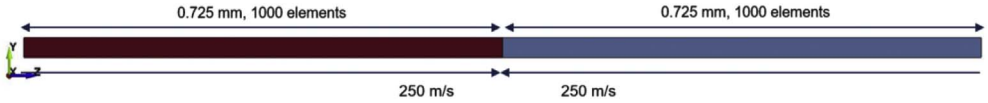

Fig. 8. Finite element model for symmetric plate impact test.

equal thickness, with each having an initial velocity of 250 m/s directed towards the centre of the model. Material model parameters given in Table 1 for aluminium were used in this simulation, with the post-processing of the stress wave formation and propagation through the thickness during the first 50 ns after the impact.

Fig. 9 shows the amplitude of the longitudinal stress vs distance at time instances of 2ns, 5ns, 10ns and 20ns after impact. A two-wave structure was formed, with the precursor having an amplitude initially levelled with the trailing shock front, before decaying over short timescales to the HEL levels. This behaviour is believed to be caused by the initial mobile dislocation density being insufficient to dissipate the strong shear stress, with the continued generation of mobile dislocations during propagation explaining the decay. This explanation is confirmed in the numerical experiment run with the increased initial value of mobile dislocations, which results in the lower precursor amplitude that is decaying faster. These results are not included in the paper.

3.3. Application of the material model to BCC single crystal metals

Evolution equations used in the material model developed in this work have been primarily used for fcc single crystal metals. However, the model has also been applied in the simulation of the plate impact tests with single crystal tantalum (bcc crystal), and validated against the experimental data published in (Whiteman et al., 2014).

In addition to extension of the material model to account for 48 bcc slip systems, this investigation included determination of nine material parameters, required for the plasticity part of the model. Five of these parameters are physical material properties available in the open literature (Steinberg, 1991). The remaining four parameters, being Y_0, A_I, k_g and V_I, required fitting to the available experimental data for rear surface velocity. Following extensive parametric investigation, it was observed that the first two parameters are sensitive to the height and form of the precursor. The V_I parameter controls the release. The set of material parameters used in the simulation tests is given in Table 3. Gruneisen equation of state parameters for tantalum are presented in Table 4.

Single crystal tantalum simulation programme consisted of three plate impact tests, conducted with a 4 mm thick target plate,

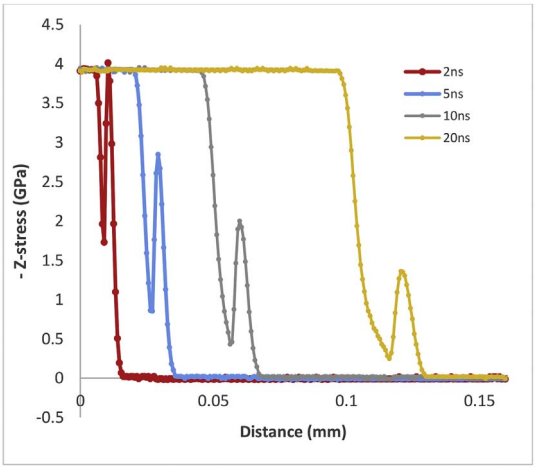

Fig. 9. Longitudinal stress vs distance in the target plate 2ns, 5ns, 10ns and 20 ns after the impact.

Table 3
Material model parameters used for the single crystal tantalum in the simulations of the plate impact tests.

Model parameter	Tantalum
E	186 GPa
G	69 GPa
ν	0.34
ρ_0	10^7 cm^{-2}
k_g	1×10^{18} J^{-1}
k_a	10
A_I	0.1
V_I	1 m/s
θ	255 K
Y_0	800 MPa
m_0	10^{-15}
a	3.306 Å

Table 4
Gruneisen equation of state parameters for tantalum (Steinberg, 1991).

Equation of state parameter	Tantalum
Velocity curve intercept, C	0.341 cm/μs
First slope coefficient, S_1	1.20
Gruneisen coefficient, γ_0	1.67
First order volume correction coefficient, a	0.42

impacted by a 3 mm flyer plate at impact velocity of 726 m/s. Impact tests were conducted along three crystallographic directions: [100], [110] and [111].

Rear surface velocity curves for the plate impact tests are compared to the experimental data (Whiteman et al., 2014) from Fig. 10 to Fig. 12. For all impact directions, the amplitude of the precursor velocity calculated in the simulations matches that of the experimental data. There is a discontinuity in the experimental data set in Fig. 10, at the time of the precursor pulse arrival at the rear surface. This discontinuity is explained in (Whiteman et al., 2014) as a temporary malfunction of the equipment used in the experiment. Nevertheless, the steep rise in velocity caused by the shock front successfully reproduces the same peak velocities as observed experimentally.

The shock front velocity obtained in the simulation of impact in [100] direction given in Fig. 10, shows a good agreement with the experimental results. The material model overestimates velocity of the shock front for impact in [110] and [111] directions, with the discrepancy between 1% and 3%. This discrepancy can well be a consequence of the assumptions made within the material model: Equation (10) is used with isotropic material constants and does not account for directional dependency of the parameters Y_0 and A_I. Equally, error in the fitting of material parameters could not be ruled out due the fitting of material parameters done with the experimental data for [100] impact. Lastly, the discrepancy could be a limitation of the current form of the model due to additional complexities of dislocation motion in bcc metals which may need to be taken into account.

Table 5
Slip system groups shown in Fig. 14.

Slip systems	Group
[1 -1 1] (0 1 1), [1 -1 1] (1 1 0), [1 1 1] (0 -1 1), [1 1 1] (-1 1 0)	Slip Systems A
[1 1 -1] (0 1 1), [-1 1 1] (1 1 0), [-1 1 1] (0 -1 1), [1 1 -1] (-1 1 0)	Slip Systems B
[1 1 -1] (1 1 2), [-1 1 1] (1 -1 2), [-1 1 1] (2 1 1), [1 1 -1] (2 -1 1)	Slip Systems C
[1 -1 1] (-1 1 2), [1 1 1] (1 1 -2), [1 1 1] (-2 1 1), [1 -1 1] (2 1 -1)	Slip Systems D
[1 -1 1] (1 2 1), [1 1 1] (1 -2 1)	Slip Systems E
[1 1 -1] (-1 2 1), [-1 1 1] (1 2 -1)	Slip Systems F
[1 1 -1] (1 2 3), [-1 1 1] (1 -2 3), [-1 1 1] (3 2 1), [1 1 -1] (3 -2 1)	Slip Systems G
[1 -1 1] (-1 2 3), [1 1 1] (1 2 -3), [1 1 1] (-3 2 1), [1 -1 1] (3 2 -1)	Slip Systems H
[-1 1 1] (3 1 2), [1 1 -1] (3 -1 2), [1 1 -1] (2 1 3), [-1 1 1] (2 -1 3)	Slip Systems I
[1 -1 1] (2 3 1), [1 1 1] (2 -3 1), [1 -1 1] (1 3 2), [1 1 1] (1 -3 2)	Slip Systems J
[1 1 -1] (-2 3 1), [-1 1 1] (2 3 -1), [1 1 -1] (-1 3 2), [-1 1 1] (1 3 -2)	Slip Systems K

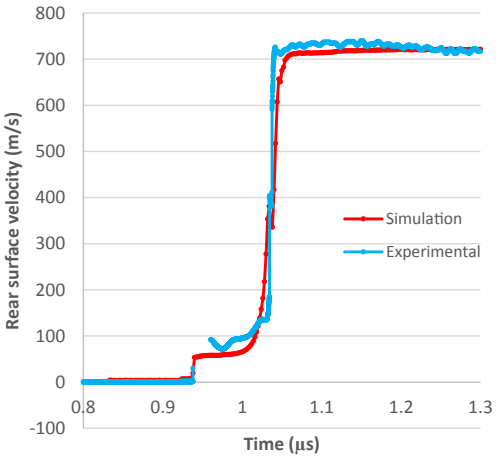

Fig. 10. Rear surface velocity obtained at the back of a single crystal tantalum plate impacted along the [100] direction at 726 m/s.

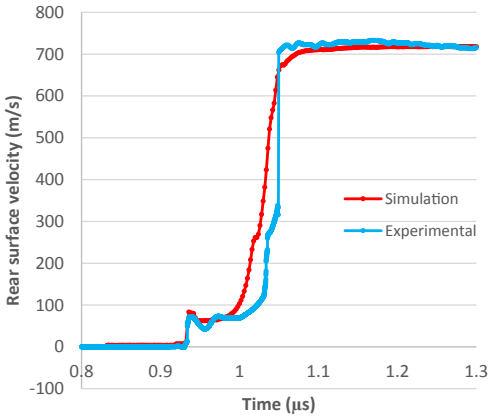

Fig. 11. Rear surface velocity of 4 mm single crystal tantalum target plate impacted by a 3 mm tantalum flyer at 726 m/s along the [110] direction.

An interesting feature of the simulation results is successful prediction of the kink, which was observed in the sharp rise of the rear surface velocity profile in all test cases considered here. These kinks were also observed in experiments on the shock loaded tantalum published in (Ding and Asay, 2011; Asay et al., 2011). Although these kinks are different is shape and appear at different time instances, they are captured with a good degree of accuracy by the material model. Analysis of the nodal velocity and stress time history in Fig. 13, obtained in an element near the rear surface, shows that the kink in the velocity curve is related to the temporary drop in the magnitude of the z-stress component. The stress drop occurs when the density of mobile dislocations and the velocity of mobile dislocations on certain slip systems begins to grow, as shown in Fig. 14 and Fig. 15, respectively. This can explain the temporary drop in z-stress as the extra mobile dislocations are generated, which correspond to the evolution of plastic strain and

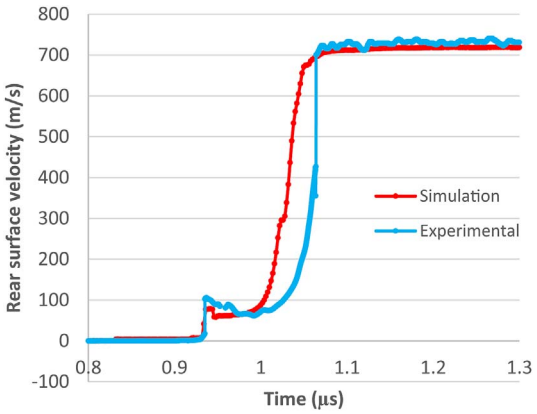

Fig. 12. Rear surface velocity of 4 mm single crystal tantalum target plate impacted by a 3 mm tantalum flyer at 726 m/s along the [111] direction.

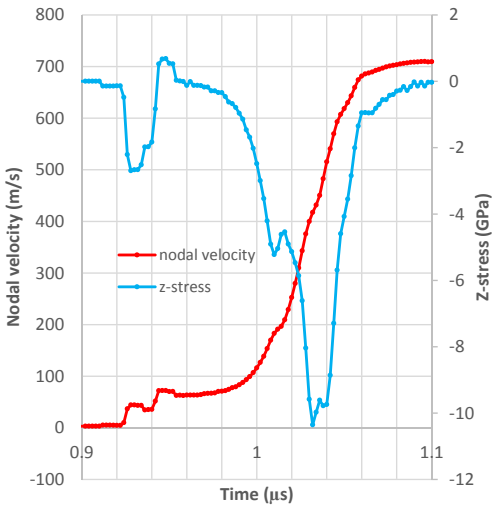

Fig. 13. Nodal velocity vs z-stress in an element near to the rear surface.

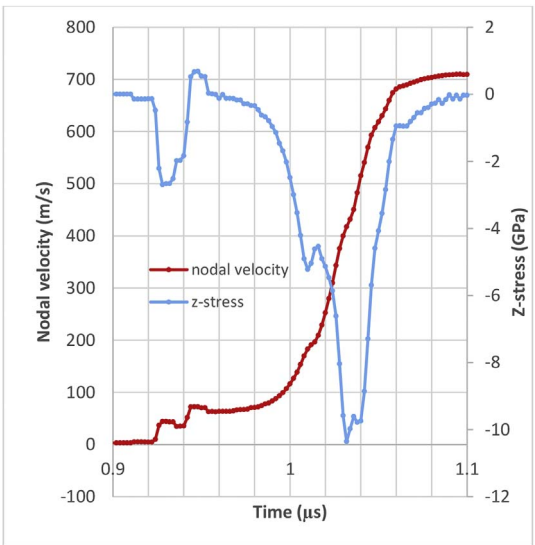

Fig. 14. Mobile dislocation density of the slip system groups defined in Table 5 plotted alongside the z-stress component.

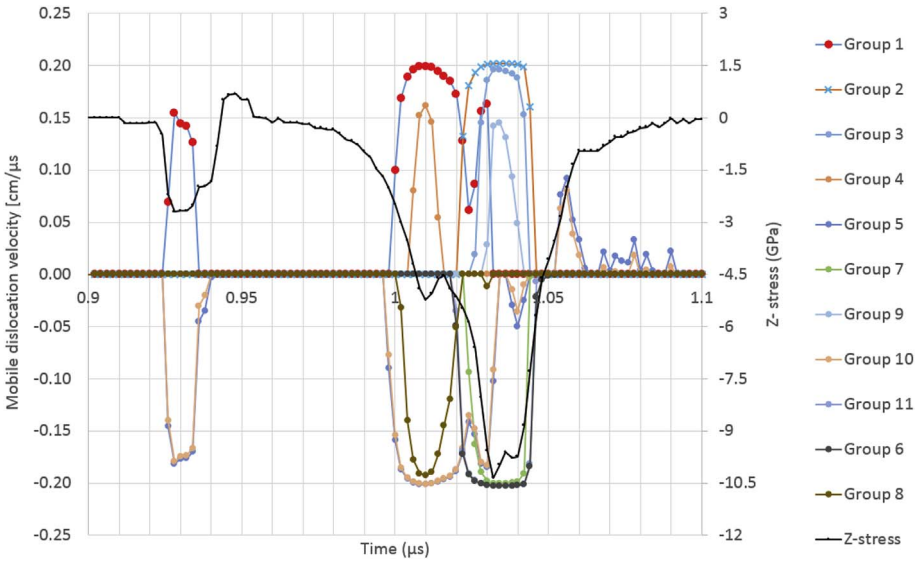

Fig. 15. Mobile dislocation velocities of the slip system groups defined in Table 5 plotted alongside the z-stress component.

increase in the dissipated energy compared to the previous time instance. Similar analysis for the [100] and [111] loading directions show the same characteristics.

Despite the discussed discrepancies between the simulation and experimental data, the main features of the experimental curves are reproduced in the simulations. The amplitude of the precursor acceleration is captured accurately, with the initial overshoot observed in the case of the [110] and [111] impact directions. The experimentally observed kink in the shock acceleration is correctly predicted in all the simulations, despite their unique character given in terms of the shape and the intensity of the kink. Further, the magnitude of rear surface velocity at which these features are observed shows a good agreement between the simulation and experimental data. Finally, for all three test cases the maximum rear surface velocity is correctly predicted.

4. Conclusions

The outlined dislocation based plasticity model has been extended to 3D and successfully implemented in LLNL-DYNA3d hydrocode and is coupled with a vector equation of state, which allows for application of the model in the orthotropic material formulation. Validation of the model has been achieved for fcc metals, using plate impact tests for both aluminium and copper specimens, with good agreement between numerically obtained and experimentally observed data.

Based on the considered range of loading rates, the material model captures the key features of the material behaviour during the shock formation and propagation through the material, with the reproduced amplitude and decay of the precursor wave. It is confirmed that the overshoot is due to the initial density of mobile dislocations being insufficient to fully dissipate the shear stress.

As a part of model validation plate impact test of a single crystal tantalum (bcc crystal structure) were simulated. The simulation results capture the main features of the material response observed experimentally, however quantitative analysis of the results revealed certain discrepancies, which can be attributed to either the constitutive relations being limited in modelling dislocation motion in bcc metals or lack of material parameters, i.e. parameter fitting of the available experimental results.

Acknowledgement

The authors would like to acknowledge that this work was financially supported by AWE.

References

Asay, J.R., Vogler, T.J., Ao, T., Ding, J.L., 2011. Dynamic yielding of single crystal Ta at strain rates of ~5 10 5/s. J. Appl. Phys. 109.

Austin, R.A., McDowell, D.L., 2012. Parameterization of a rate-dependent model of shock-induced plasticity for copper, nickel, and aluminum. Int. J. Plast. 32–33, 134–154.

Austin, R.A., McDowell, D.L., 2011. A dislocation-based constitutive model for viscoplastic deformation of fcc metals at very high strain rates. Int. J. Plast. 27, 1–24.

Banerjee, B., Bhawalkar, A.S., 2008. An extended mechanical threshold stress plasticity model: modeling 6061-T9 aluminum alloy. J. Mech. Mater. Struct. 3, 391–424.

Colvin, J.D., Minich, R.W., Kalantar, D.H., 2009. A model for plasticity kinetics and its role in simulating the dynamic behavior of Fe at high strain rates. Int. J. Plast.

25, 603–611.
Ding, J.L., Asay, J.R., 2011. Modeling of the dynamic inelasticity of tantalum single crystal under ramp wave loading. J. Appl. Phys. 109.
Follansbee, P.S., Kocks, U.F., 1988. A constitutive description of the deformation of copper based on the use of the mechanical threshold stress as an internal state variable. Acta Metall. 36, 81–93.
Groh, S., Marin, E.B., Horstemeyer, M.F., Zbib, H.M., 2009. Multiscale modeling of the plasticity in an aluminum single crystal. Int. J. Plast. 25, 1456–1473.
Hansen, B.L., Beyerlein, I.J., Bronkhorst, C.A., Cerreta, E.K., Dennis-Koller, D., 2013a. A dislocation-based multi-rate single crystal plasticity model. Int. J. Plast. 44, 129–146.
Hansen, B.L., Carpenter, J.S., Sintay, S.D., Bronkhorst, C.A., McCabe, R.J., Mayeur, J.R., Mourad, H.M., Beyerlein, I.J., Mara, N.A., Chen, S.R., Gray, G.T., 2013b. Modeling the texture evolution of Cu/Nb layered composites during rolling. Int. J. Plast. 49, 71–84.
Johnson, G.R., Cook, W.H., 1983. A constitutive model and data for metals subjected to large strains, high strain rates and high temperatures. In: Proceedings of the 7th International Symposium of Ballistics, pp. 541–547.
Kanel, G.I., Razorenov, S.V., Utkin, A.V., Baumung, K., 1996. Experimental profiles of shock waves. In: Preprint of Scientific Association IVTAN of RAS.
Kanel, G.I., Razorenov, S.V., Baumung, K., Singer, J., 2001. Dynamic yield and tensile strength of aluminum single crystals at temperatures up to the melting point. J. Appl. Phys. 90, 136–143.
Khan, A.S., Liu, J., Yoon, J.W., Nambori, R., 2015. Strain rate effect of high purity aluminum single crystals: experiments and simulations. Int. J. Plast. 67, 39–52.
Khan, A.S., Liu, J., 2016. A deformation mechanism based crystal plasticity model of ultrafine-grained/nanocrystalline FCC polycrystals. Int. J. Plast. 86, 56–69.
Kosevich, A.M., 1965. Dynamical theory of dislocations. Sov. Phys. Usp. 7, 837–854.
Krasnikov, V.S., Kuksin, A.Y., Mayer, A.E., Yanilkin, A.V., 2010. Plastic deformation under high-rate loading: the multiscale approach. Phys. Solid State 52, 1386–1396.
Krasnikov, V.S., Mayer, A.E., Yalovets, A.P., 2011. Dislocation based high-rate plasticity model and its application to plate-impact and ultra short electron irradiation simulations. Int. J. Plast. 27, 1294–1308.
Li, D., Zbib, H., Sun, X., Khaleel, M., 2014. Predicting plastic flow and irradiation hardening of iron single crystal with mechanism-based continuum dislocation dynamics. Int. J. Plast. 52, 3–17.
Liu, J., 2004. Dyna3D: a Nonlinear, Explicit, Three-dimensional Finite Element Code for Solid and Structural Mechanics. 1999.
Luscher, D.J., Mayeur, J.R., Mourad, H.M., Hunter, A., Kenamond, M.A., 2016. Coupling continuum dislocation transport with crystal plasticity for application to shock loading conditions. Int. J. Plast. 76, 111–129.
Malygin, G.A., 1999. Dislocation self-organization processes and crystal plasticity. Phys. Usp. 42, 887–916.
Mandel, J., 1974. Thermodynamics and Plasticity. Foundations of Continuum Thermodynamics, pp. 283–304.
Mandel, J., 1972. Plasticite Classique Et Viscoplasticite. Springer, Vienna CISM course no. 97.
Mayer, A.E., Khishchenko, K.V., Levashov, P.R., Mayer, P.N., 2013. Modeling of plasticity and fracture of metals at shock loading. J. Appl. Phys. 113.
Mayer, A.E., Mayer, P.N., Krasnikov, V.S., Voronin, D.S., 2015. Multi-scale model of the dynamic fracture of molten and solid metals. J. Phys. Conf. Ser. 653.
Mayeur, J.R., Mourad, H.M., Luscher, D.J., Hunter, A., Kenamond, M.A., 2016. Numerical implementation of a crystal plasticity model with dislocation transport for high strain rate applications. Model. Simul. Mater. Sci. Eng. 24.
Meyers, M.A., 1994. Dynamic Behaviour of Materials. John Waley & Sons, Inc., New York.
Qi, C., Wang, M., Qian, Q., 2009. Strain-rate effects on the strength and fragmentation size of rocks. Int. J. Impact Eng. 36, 1355–1364.
Reese, S., Vladimirov, I.N., 2008. Anisotropic modelling of metals in forming processes. In: IUTAM Symposium on Theoretical, Computational and Modelling Aspects of Inelastic Media 11. pp. 175–184.
Steinberg, D.J., 1991. Equation of State and Strength Properties of Selected Materials. UCRL-MA-106439.
Steinberg, D.J., Cochran, S.G., Guinan, M.W., 1980. A constitutive model for metals applicable at high-strain rate. J. Appl. Phys. 51, 1498–1504.
Steinberg, D.J., Lund, C.M., 1989. A constitutive model for strain rates from 10-4 to 106 s-1. J. Appl. Phys. 65, 1528–1533.
Suzuki, T., Takeuchi, S., Yoshinaga, H., 1991. Dislocation Dynamics and Plasticity. Springer-Verlag, Berlin; London.
Vignjevic, R., Campbell, J.C., Bourne, N.K., Djordjevic, N., 2008. Modeling shock waves in orthotropic elastic materials. J. Appl. Phys. 104.
Vignjevic, R., Djordjevic, N., Panov, V., 2012. Modelling of dynamic behaviour of orthotropic metals including damage and failure. Int. J. Plast. 38, 47–85.
Vladimirov, I.N., Pietryga, M.P., Reese, S., 2009. Anisotropic finite elastoplasticity with nonlinear kinematic and isotropic hardening and application to sheet metal forming. Int. J. Plast. 26, 659–687.
Whiteman, G., Case, S., Millett, J.C.F., 2014. Planar shock compression of single crystal tantalum from 6-23 GPa. J. Phys. Conf. Ser. 500.
Yanilkin, A.V., Krasnikov, V.S., Kuksin, A.Y., Mayer, A.E., 2014. Dynamics and kinetics of dislocations in Al and Al–Cu alloy under dynamic loading. Int. J. Plast. 55, 94–107.
Zerilli, F.J., Armstrong, R.W., 1987. Dislocation-mechanics-based constitutive relations for material dynamics calculations. J. Appl. Phys. 61, 1816–1825.
Zhakhovsky, V.V., Demaske, B.J., Inogamov, N.A., Khokhlov, V.A., Ashitkov, S.I., Agranat, M.B., Oleynik, I.I., 2012. Super-elastic response of metals to laser-induced shock waves. AIP Conf. Proc. 1464, 102–112.